

ViP3D: End-to-end Visual Trajectory Prediction via 3D Agent Queries

Junru Gu^{1*} Chenxu Hu^{1*} Tianyuan Zhang^{2,3} Xuanyao Chen^{2,4}

Yilun Wang⁵ Yue Wang⁶ Hang Zhao^{1,2†}

¹IIIS, Tsinghua University ²Shanghai Qi Zhi Institute

³CMU ⁴Fudan University ⁵Li Auto ⁶MIT

Abstract: Existing autonomous driving pipelines separate the perception module from the prediction module. The two modules communicate via hand-picked features such as agent boxes and trajectories as interfaces. Due to this separation, the prediction module only receives partial information from the perception module. Even worse, errors from the perception modules can propagate and accumulate, adversely affecting the prediction results. In this work, we propose ViP3D, a visual trajectory prediction pipeline that leverages the rich information from raw videos to predict future trajectories of agents in a scene. ViP3D employs sparse agent queries throughout the pipeline, making it fully differentiable and interpretable. Furthermore, we propose an evaluation metric for this novel end-to-end visual trajectory prediction task. Extensive experimental results on the nuScenes dataset show the strong performance of ViP3D over traditional pipelines and previous end-to-end models.¹

Keywords: Trajectory Prediction, Autonomous Driving, End-to-End Learning

1 Introduction

Safe autonomous systems require understanding future behaviors of agents, so that the autonomous vehicles could navigate the world safely. Therefore, trajectory prediction has attracted a lot of attention in the recent years [1, 2, 3, 4, 5, 6, 7, 8, 9]. The common practice of autonomous driving software stack is to separate it into a “perception-prediction-planning” pipeline, where the interface between the perception and the prediction module is often defined by hand-picked agent features, such as historical trajectories, agent types, agent sizes, *etc.* Such construction leads to a loss of perceptual information that is useful for trajectory prediction. For example, tail lights and brake lights indicate vehicles’ intention clearly, but such information is completely ignored in the existing pipelines. In addition, with the separation of perception and prediction, errors are accumulated and cannot be cured in later stages. For example, historical trajectories used by trajectory predictors come from an upstream perception module, which inevitably contains errors, leading to a drop in the trajectory prediction performance. Designing a trajectory predictor that is robust to upstream output errors is a non-trivial task [10].

To that end, recent works such as IntentNet [11], FaF [12], PnPNet [13] propose end-to-end models for trajectory prediction. These models heavily rely on convolutional neural networks, using feature maps and heatmaps as their intermediate representations. However, these pipelines still suffer from non-differentiable post-processing steps, e.g., non-maximum suppression in detection and object association in tracking.

To address all these challenges, we propose a novel end-to-end model, dubbed **ViP3D** (Visual trajectory Prediction via **3D** agent queries). ViP3D directly leverages visual features from raw videos

^{*}Equal contribution.

[†]Corresponding to: hangzhao@mail.tsinghua.edu.cn

¹Project page: <https://tsinghua-mars-lab.github.io/ViP3D>

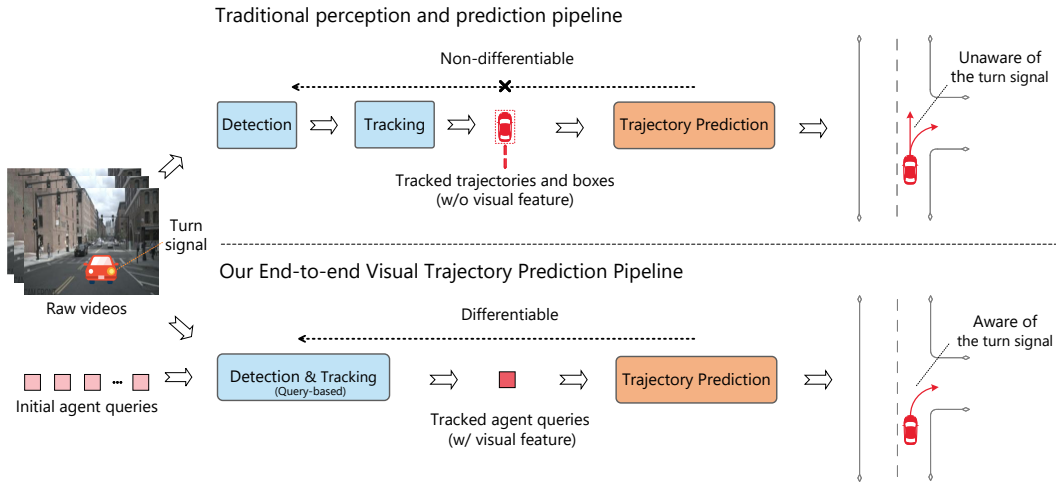


Figure 1: Comparison of a traditional multi-stage cascaded pipeline and ViP3D. The traditional pipeline involves multiple non-differentiable modules, e.g., detection, tracking, and prediction. ViP3D takes multi-view videos as input and generates predicted trajectories in an end-to-end manner, which can effectively leverage visual information such as turning signals of vehicles.

of surrounding cameras to represent agents in the scene in a sparse manner. Specifically, ViP3D is a pipeline composed of a query-based tracker and a trajectory predictor, with a set of sparse agent queries passing information throughout the pipeline. The tracker takes streaming video frames as input, together with a set of agent queries. These queries extract agent-level visual features, model the relationship between agents, and learn agent dynamics across frames. The trajectory predictor consumes these agent queries together with high-definition semantic maps to produce K possible future trajectories for each agent. Meanwhile, we find that classical trajectory prediction metrics do not apply to our end-to-end visual trajectory prediction pipeline, so we develop a new evaluation metric, **End-to-end Prediction Accuracy (EPA)**, which scores predicted trajectories against ground-truth trajectories while comprehensively considering the accuracy of both perception and prediction.

In summary, the novelty of ViP3D is three-fold:

1. ViP3D is the first **vision-based** approach to predict future trajectories of agents for autonomous driving. Compared with hand-picked features like historical trajectories and agent sizes, visual features can implicitly encode richer, detailed, fine-grained information which is useful for the trajectory prediction task.
2. The novel agent query-based design makes ViP3D **fully differentiable**, thus avoiding error accumulation in the pipeline. Of note, this is different from recent end-to-end models [13] which jointly train multiple modules with intermediate discrete operations such as non-maximum suppression (NMS) and object association.
3. ViP3D explicitly models **instance-wise** agent detection, tracking and prediction, making it more interpretable and debuggable compared to recent heatmap-based motion prediction methods [14].

Experiments on the public nuScenes dataset [15] show that ViP3D significantly outperforms a wide variety of baselines and recent end-to-end methods on the visual trajectory prediction task.

2 Related Work

3D Detection. There are a great number of works on 3D object detection and tracking from point clouds [16, 17, 18]. In this paper, we focus on 3D detection and tracking from cameras. Monodis [19] and FCOS3D [20] learns a single-stage object detector with instance depth and 3D pose predictions on monocular images. Pseudo-LiDAR [21] first predicts depth for each image pixel, then lifts them into the 3D space, and finally employs a point cloud based pipeline to perform 3D detection. DETR3D [22] designs a sparse 3D query-based detection model that maps queries onto 2D multi-view images to extract features. BEVFormer [23] further proposes a dense query-based detection model.

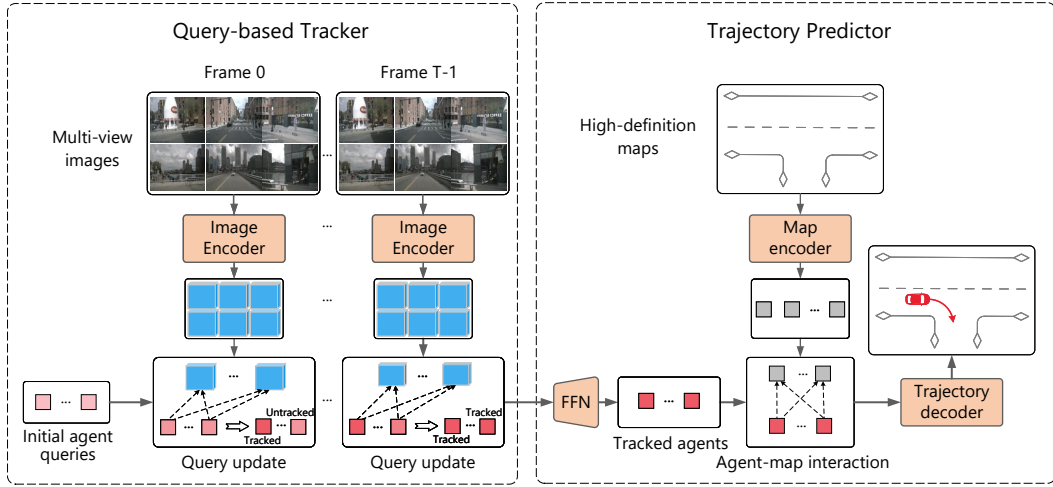


Figure 2: The architecture of ViP3D. A sequence of multi-view images are fed into the query-based tracker to obtain tracked agent queries containing visual features. The agent queries further interact with HD map features, and are sent into the trajectory decoder to output predicted trajectories.

3D Tracking. The majority of 3D tracking approaches follow the tracking-by-detection pipeline [24, 25]. These methods first detect 3D objects, then associate existing tracklets with the new detections. CenterTrack [26, 27] uses two consecutive frames to predict the speed of each detection box, then performs association using only ℓ_2 distances of the boxes. Samuel *et al.* [28] uses PMBM filter to estimate states of tracklets and match them with new observations. DEFT [29] uses a learned appearance matching network for association, together with an LSTM estimated motion to eliminate implausible trajectories. QD3DT [30] uses cues from depth-ordering and learns better appearance features via contrastive learning. MUTR3D [31] introduces track queries to model objects that appear in multiple cameras across multiple frames.

Trajectory Prediction. Most trajectory prediction works focus on modeling the uncertainty of unknown intents and behaviors of agents. Variety loss is a regression-based method that only optimizes the closest predicted trajectory during training. Modeling uncertainty using latent variables [32, 33, 34, 35] is another popular approach, which predicts different future trajectories by randomly sampling from the latent variables. Goal-based methods recently achieve outstanding performance by first predicting intentions of agents, such as the endpoint of trajectories [7, 9, 36, 37], lanes to follow [38, 39, 40], and then predicting future trajectories conditioning on these goals.

End-to-End Perception and Prediction. In the last couple of years, there has been growing interest in jointly optimizing detection, tracking, and prediction. FaF [12] employs a single convolutional neural network to detect objects from LiDAR point clouds, and forecast their corresponding future trajectories. IntentNet [11] adds high-level intention output to this framework. More recently, Phillips *et al.* [41] further learns localization together with perception and prediction. FIERY [14] predicts future BEV occupancy heatmaps from visual data directly. Mostly related to our work is PnPNet [13], which explicitly models tracking in the loop. Our method is related to these methods in the sense that we also perform end-to-end prediction based on sensor inputs. However, they all rely on BEV feature maps or heatmaps as their intermediate representation, which leads to unavoidable non-differentiable operation while going from dense feature maps to instance-level features, such as non-maximum suppression (NMS) in detection, and association in tracking. Our method, on the other hand, employs sparse agent queries as representation throughout the model, greatly improving the differentiability and interpretability.

3 Method

ViP3D aims to address the trajectory prediction problem from raw videos in an end-to-end fashion. Concretely, given multi-view videos and HD maps, ViP3D predicts future trajectories of all agents in the scene. The overall pipeline of ViP3D is shown in Figure 2. First, we apply a query-based tracker to process multi-view videos from surrounding cameras to obtain tracked agent queries with visual features. The visual features in the agent queries capture the motion dynamics and visual characteristics of the agents and the relationships between agents. After that, a trajectory predictor

takes the tracked agent queries as input and associates them with HD map features, and finally outputs predicted trajectories.

3.1 Query-based Tracker

As shown in Figure 2, the query-based tracker extracts visual features from raw videos of surrounding cameras. Specifically, for each frame, we follow DETR3D [22] to extract image features. For temporal feature aggregation, we follow MOTR [42] to design a query-based tracker, which consists of two key steps: query feature update and query supervision. Agent queries are updated across time to model the motion dynamics of agents.

3.1.1 Query Feature Update

In ViP3D, each agent query corresponds to at most one agent that appeared in the scene. We use \mathbf{Q} to denote a set of agent queries, which are initialized as learnable embeddings with 3D reference points. At each time step, we first extract 2D image features of surrounding cameras via ResNet50 [43] and FPN [44]. Then we project the 3D reference points of agent queries onto the 2D coordinates of multi-view images using camera intrinsic and extrinsic transformation matrices. Finally, we sample the corresponding image features to update the agent queries via cross attention: $\mathbf{Q}_t = \mathbf{Q}\mathbf{W}^Q, \mathbf{K} = \mathbf{L}\mathbf{W}^K, \mathbf{V} = \mathbf{L}\mathbf{W}^V, \mathbf{A}(\mathbf{Q}_t, \mathbf{K}, \mathbf{V}) = \text{softmax}\left(\frac{\mathbf{Q}_t\mathbf{K}^\top}{\sqrt{d_k}}\right)\mathbf{V}, \mathbf{Q} = \text{FFN}_{\text{upd}}(\mathbf{Q}, \mathbf{A}(\mathbf{Q}_t, \mathbf{K}, \mathbf{V}))$, where $\mathbf{W}^Q, \mathbf{W}^K, \mathbf{W}^V \in \mathbb{R}^{d_h \times d_k}$ are the matrices for linear projection, $t \in \{1, \dots, T\}$ is the current time step, d_k is the dimension of query / key / value vectors, and \mathbf{L} is the sampled 2D image features. FFN_{upd} is a two-layer MLP that updates the feature of the queries.

3.1.2 Query Supervision

Since each agent query corresponds to at most one agent, supervision is required at each time step to make sure each query extracts features of the same agent across different historical frames. There are two types of queries. One are the matched queries that have been associated with agents before this time step. The other are the empty queries that have not been associated with any agents. Suppose we have done association at time step $t - 1$, and now we perform association at time step t . For the matched queries, we assign the same agents to them as before: $\mathbf{Q}_{\text{matched}} \cong \mathcal{A}_{\text{old}}$, where \mathcal{A}_{old} denotes the agents appeared at time step $t - 1$. If an agent disappeared at time step t , we assign an empty label to the query which is associated with that agent at time step $t - 1$. For the unmatched queries, we perform a bipartite matching between the unmatched queries and the new agents \mathcal{A}_{new} appeared at time step t : $\mathbf{Q}_{\text{empty}} \cong \mathcal{A}_{\text{new}}$.

To perform the bipartite matching, we utilize a query decoder that outputs the center coordinates of each query at time step t . The pair-wise matching cost [45] between ground truth y_i and a prediction $\hat{y}_{\sigma(i)}$ for the bipartite matching is: $\mathcal{L}_{\text{match}}(y_i, \hat{y}_{\sigma(i)}) = -\mathbb{1}_{\{c_i \neq \emptyset\}}\hat{p}_{\sigma(i)}(c_i) + \mathbb{1}_{\{c_i \neq \emptyset\}}\mathcal{L}_{\text{box}}(b_i, \hat{b}_{\sigma(i)})$, where c_i is the target class label, b_i is the target box, $\hat{b}_{\sigma(i)}$ and $\hat{p}_{\sigma(i)}(c_i)$ are the predicted box and predicted probability of class c_i , respectively.

After the bipartite matching, we get the optimal assignment $\hat{\sigma}$. We compute the query classification loss \mathcal{L}_{cls} and query coordinate regression loss $\mathcal{L}_{\text{coord}}$ as follows:

$$\mathcal{L}_{\text{cls}} = \sum_{i=1}^N -\log \hat{p}_{\hat{\sigma}(i)}(c_i), \quad \mathcal{L}_{\text{coord}} = \sum_{i=1}^N \mathbb{1}_{\{c_i \neq \emptyset\}}\mathcal{L}_{\text{box}}(b_i, \hat{b}_{\hat{\sigma}(i)}), \quad (1)$$

where \mathcal{L}_{box} is the ℓ_1 loss for bounding box parameters.

3.2 Trajectory Predictor

Most existing trajectory prediction methods can be divided into three components: agent encoding, map encoding, and trajectory decoding. After query-based tracking, we obtain tracked agent queries, which can be viewed as agent features obtained by agent encoding. Therefore, the remaining tasks are map encoding and trajectory decoding.

3.2.1 Map Encoder

For an accurate trajectory prediction, the use of HD semantic maps is crucial since they include detailed road information, such as lane types, road boundaries and traffic signs. HD maps are represented by vectorized spatial coordinates of map elements and the topological relations between them. To encode this information, we adopt a popular vectorized encoding method VectorNet [46]. Compared with rasterized encoding methods which render maps and agents on an image and extract image features using CNNs, vectorized encoding methods abstract all the map elements and efficiently model their spatial and topological relationships. The map encoder produces a set of map features \mathbf{M} , which further interacts with agent queries via cross attention: $\mathbf{Q} = \text{Attention}(\mathbf{Q}, \mathbf{M})$.

3.2.2 Trajectory Decoder

The trajectory decoder takes in the agent queries, and outputs K possible future trajectories for each agent. ViP3D can leverage a variety of trajectory decoding methods, such as regression-based methods [4, 47, 48, 40], goal-based methods [7] and heatmap-based methods [9, 36, 49]. For completeness, we conduct experiments on these three trajectory decoding methods. We introduce the key ideas of these methods here and leave the details in the Appendix. (1) The regression-based method, namely variety loss, predicts future trajectories based on regression. During inference, this decoder directly outputs a set of predicted trajectories. During training, we first calculate the distance between each predicted trajectory and ground truth trajectory. Then we select a predicted trajectory with the closest distance and only calculate regression loss between it and the ground truth trajectory. (2) The goal-based method first defines sparse goal anchors heuristically, and then classifies these anchors to estimate and select the goals. Finally, a trajectory is completed for each selected goal. (3) The heatmap-based method first generates a heatmap indicating the probability distribution of the goal. Then a greedy algorithm or a neural network is used to select goals from the heatmap. Finally, same as the goal-based method, the trajectories are completed.

3.3 Loss

ViP3D is trained end-to-end with query classification loss and query coordinate regression loss of the query-based tracker, and trajectory decoding loss of the trajectory predictor: $\mathcal{L} = \mathcal{L}_{\text{cls}} + \mathcal{L}_{\text{coord}} + \mathcal{L}_{\text{trajectory}}$.

3.4 A New Metric for End-to-end Visual Trajectory Prediction

End-to-end trajectory prediction from raw videos poses a new challenge in evaluation. Since historical trajectories are not used as input, there is no correspondence between predicted trajectories and ground truth trajectories, making it difficult to calculate the classical prediction metrics. Thus, we propose a new evaluation metric, End-to-end Prediction Accuracy (EPA), for trajectory prediction from raw videos. EPA finds matches between predicted trajectories and ground-truth trajectories and comprehensively considers both detection accuracy and prediction accuracy.

We denote predicted and ground truth agents as unordered sets $\hat{\mathcal{S}}$ and \mathcal{S} , respectively, where each agent is represented by agent coordinates at the current time step and K possible future trajectories. First, for each agent type c , we calculate the prediction precision between $\hat{\mathcal{S}}_c$ and \mathcal{S}_c . We define the cost between a predicted agent \hat{s} and a ground truth agent s as:

$$C_{\text{EPA}}(s, \hat{s}) = \begin{cases} \|s_0 - \hat{s}_0\|, & \text{if } \|s_0 - \hat{s}_0\| \leq \tau_{\text{EPA}} \\ \infty, & \text{if } \|s_0 - \hat{s}_0\| > \tau_{\text{EPA}} \end{cases}, \quad (2)$$

where \hat{s}_0 and s_0 indicate the coordinates of the ground truth agent and the predicted agent at the current time step, and τ_{EPA} is the threshold for matching cost. We utilize C_{EPA} to find the closest predicted agent for each ground truth agent, and take this predicted agent as a matched agent. Then the number of false-positive predicted agents is: $N_{\text{FP}} = |\hat{\mathcal{S}}| - |\hat{\mathcal{S}}_{\text{match}}|$, where $\hat{\mathcal{S}}_{\text{match}} \subset \hat{\mathcal{S}}$ is the set of predicted agents which have been matched with ground truth agents. For each matched agent, we follow the classical prediction metric and calculate minFDE (minimum final displacement error) between its predicted multiple future trajectories and the ground truth trajectory: $\text{minFDE}(\hat{s}, s) = \min_{k \in 1 \dots K} \|\hat{s}_{T_{\text{future}}}^{(k)} - s_{T_{\text{future}}}\|$, where $\hat{s}^{(k)}$ is the k -th trajectory of the matched agent \hat{s} , and T_{future} is

the final time step of the future trajectory. Now the set of predicted agents which have matched and hit a ground truth agent is $\hat{\mathcal{S}}_{\text{match, hit}} = \{\hat{\mathbf{s}} : \hat{\mathbf{s}} \in \hat{\mathcal{S}}_{\text{match}}, \min \text{FDE}(\hat{\mathbf{s}}, \mathbf{s}) \leq \tau_{\text{EPA}}\}$. Therefore, the EPA between $\hat{\mathcal{S}}_c$ and \mathcal{S}_c is defined as:

$$\text{EPA}(\hat{\mathcal{S}}_c, \mathcal{S}_c) = \frac{|\hat{\mathcal{S}}_{\text{match, hit}}| - \alpha N_{\text{FP}}}{N_{\text{GT}}}, \quad (3)$$

where N_{GT} is the number of ground truth agents, and we set penalty coefficient $\alpha = 0.5$ for all experiments. Finally, the EPA is averaged across all agent types.

4 Experiments

4.1 Dataset and Task

Dataset. We train and evaluate ViP3D on the nuScenes dataset, a large-scale driving dataset including the urban scenarios in Boston and Singapore. It contains 1000 scenes, and each scene has a duration of around 20 seconds. The full dataset has more than one million images from 6 cameras and 1.4M bounding boxes for different types of objects. Bounding boxes of objects are annotated at 2Hz over the entire dataset.

Visual Trajectory Prediction Task. Different from traditional trajectory prediction tasks, whose inputs are historical trajectories of agents. In our visual trajectory prediction task, we take raw videos from surrounding cameras as input, and the output is an unordered set of multi-modal future trajectories. During evaluation, we compute metrics between the predicted unordered set of future trajectories and the ground truth unordered set of future trajectories.

4.2 Baseline Settings

Traditional Perception and Prediction Pipeline. The traditional pipeline has independently trained tracker and trajectory predictor. In our experiment, this baseline uses the same query-based tracker and trajectory predictor as ViP3D for a fair comparison. Compared with ViP3D, the outputs of the tracker are agent attributes and states instead of agent queries. These agent attributes and states are manually-defined in common tracking tasks, and we use as many attributes as possible. They include historical trajectories, agent types, agent sizes, agent velocities, *etc.*

PnPNet. PnPNet [13] only takes LiDAR data as input, and it cannot be directly used for our visual trajectory prediction task. To compare our ViP3D with PnPNet, we use DETR3D as backbone to encode raw videos for PnPNet, and use the same query-based tracker for tracking in PnPNet. The outputs of LiDAR encoder in the original PnPNet are BEV feature maps. After replacing LiDAR encoder with DETR3D, the outputs become image features. In the original PnPNet, visual features of tracked agents are obtained by performing bilinear sampling in BEV feature maps using agent coordinates. After applying DETR3D, we obtain visual features of tracked agents by cross attention from agent coordinates to the image features obtained by DETR3D. Besides, we use the same trajectory predictor in our experiments for a fair comparison.

4.3 Evaluation and Analysis

4.3.1 Main Results

We compare our ViP3D with PnPNet and traditional perception and prediction pipeline on the nuScenes dataset. For a comprehensive comparison, we test the performance of each baseline under three different trajectory decoding methods, as shown in Table 1. We can see that ViP3D outperforms these baselines across almost all the trajectory decoding methods, indicating the effectiveness and superiority of ViP3D. It also demonstrates the benefit of directly learning from visual information with a fully differentiable approach.

4.3.2 Ablation Study

Trajectory Predictor. To better understand the necessity of visual features and end-to-end training, we compare ViP3D with different baselines. These baselines have the same architecture as

Table 1: Comparing ViP3D with PnPNet and traditional multi-stage pipeline under three different trajectory decoding methods. Classical metrics include minADE (ADE), minFDE (FDE) and Miss Rate (MR), and End-to-end Prediction Accuracy (EPA) is the proposed metric for our end-to-end setting. For each agent, 6 future trajectories with a time horizon of 6 seconds are evaluated.

Pipeline	Trajectory Decoding	Vehicle				Pedestrian			
		ADE↓	FDE↓	MR↓	EPA↑	ADE↓	FDE↓	MR↓	EPA↑
Traditional	Regression-based [47]	2.26	3.22	0.284	0.234	2.35	3.43	0.280	0.138
PnPNet [13]		2.13	2.96	0.258	0.244	2.30	3.37	0.287	0.142
ViP3D (ours)		2.14	2.92	0.254	0.253	1.96	2.77	0.238	0.199
Traditional	Goal-based [7]	2.64	4.37	0.286	0.233	2.35	3.50	0.247	0.158
PnPNet [13]		2.73	4.59	0.252	0.250	2.30	3.35	0.292	0.141
ViP3D (ours)		2.52	4.05	0.242	0.250	2.20	3.11	0.241	0.137
Traditional	Heatmap-based [36]	2.72	4.16	0.268	0.243	2.34	3.45	0.260	0.151
PnPNet [13]		2.73	4.17	0.255	0.249	2.35	3.58	0.315	0.127
ViP3D (ours)		2.62	3.94	0.220	0.268	2.04	2.90	0.215	0.159

Table 2: Ablation study on the inputs of trajectory predictor. Trajectory decoding is default to regression-based method.

	Interface		Differentiable	EPA↑
	Traj.	Visual feat.		
	✓	✗	✗	0.186
	✗	✓	✗	0.210
	✓	✓	✗	0.211
ViP3D	✗	✓	✓	0.226

Table 3: Ablation study comparing the performance of the tracker in ViP3D and the one trained separately.

Tracker	AMOTA	AMOTP	Recall
Separately-trained	0.216	1.616	0.358
ViP3D	0.217	1.625	0.363

ViP3D except for the interface between the tracker and the trajectory predictor. We use the default regression-based method for trajectory decoding. EPA averaged over vehicles and pedestrians is used to compare their performance on visual trajectory prediction task. Results are shown in Table 2. It can be seen that *Trajectory* + *Visual feature* outperforms *Trajectory*, demonstrating that the visual features provide more fine-grained and detailed information to improve prediction performance. In addition, *Visual feature* surpasses *Trajectory* and is very close to *Trajectory* + *Visual feature*, which shows that the visual features contain almost all the information that the trajectories can provide. ViP3D surpasses *Trajectory* and *Trajectory* + *Visual feature*, demonstrating that end-to-end learning is helpful in avoiding the error accumulation problem in the multi-stage pipeline.

Tracker. We also compare the tracking performance between a separately trained tracker and the tracker of our end-to-end trained ViP3D. These trackers have the same architecture, only the training strategies differ. Results in Table 3 show that the our end-to-end trained tracker slightly outperforms the separately trained tracker.

4.3.3 Qualitative Results

We provide an example of the predicted results by ViP3D in Figure 3. As the figure shows, ViP3D can detect agents in the scene accurately together with their future trajectories. More visualizations can be found in the Appendix.

5 Conclusion

We present ViP3D, a fully differentiable approach to predict future trajectories of agents from multi-view videos. It leverages the rich visual information from the raw sensory input, and also avoids the error accumulation problem in the traditional pipeline. Moreover, by operating in a sparse manner with agent queries, ViP3D models agent instances explicitly, making the pipeline interpretable and debuggable.

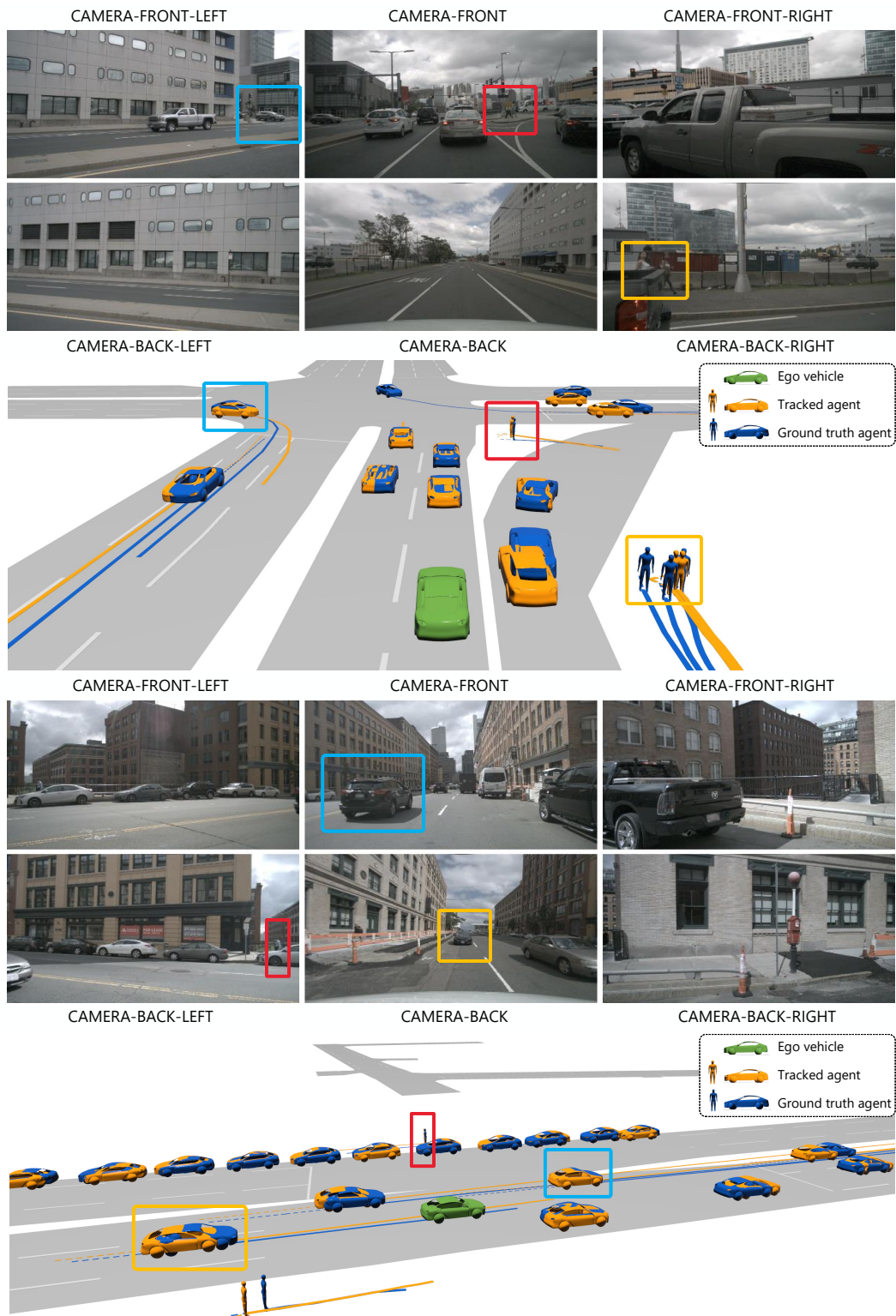


Figure 3: Qualitative results of ViP3D for end-to-end trajectory prediction. Agents with the same identity are enclosed by boxes of the same color. The green vehicle is the ego agent. The blue and orange agents indicate ground-truth and tracked agents, respectively. The blue and orange curves indicate ground-truth and predicted future trajectories of agents, respectively. For each agent, only the predicted trajectory with the highest probability is drawn.

References

- [1] H. Cui, V. Radosavljevic, F.-C. Chou, T.-H. Lin, T. Nguyen, T.-K. Huang, J. Schneider, and N. Djuric. Multimodal trajectory predictions for autonomous driving using deep convolutional networks. In *2019 International Conference on Robotics and Automation (ICRA)*, pages 2090–2096. IEEE, 2019.
- [2] N. Lee, W. Choi, P. Vernaza, C. B. Choy, P. H. Torr, and M. Chandraker. Desire: Distant future prediction in dynamic scenes with interacting agents. In *Proceedings of the IEEE Conference on Computer Vision and Pattern Recognition*, pages 336–345, 2017.
- [3] Y. Yuan and K. M. Kitani. Diverse trajectory forecasting with determinantal point processes. In *International Conference on Learning Representations*, 2019.
- [4] A. Gupta, J. Johnson, L. Fei-Fei, S. Savarese, and A. Alahi. Social gan: Socially acceptable trajectories with generative adversarial networks. In *Proceedings of the IEEE Conference on Computer Vision and Pattern Recognition*, pages 2255–2264, 2018.
- [5] Y. Chai, B. Sapp, M. Bansal, and D. Anguelov. Multipath: Multiple probabilistic anchor trajectory hypotheses for behavior prediction. *arXiv preprint arXiv:1910.05449*, 2019.
- [6] T. Phan-Minh, E. C. Grigore, F. A. Boulton, O. Beijbom, and E. M. Wolff. Covernet: Multi-modal behavior prediction using trajectory sets. In *Proceedings of the IEEE/CVF Conference on Computer Vision and Pattern Recognition*, pages 14074–14083, 2020.
- [7] H. Zhao, J. Gao, T. Lan, C. Sun, B. Sapp, B. Varadarajan, Y. Shen, Y. Shen, Y. Chai, C. Schmid, et al. Tnt: Target-driven trajectory prediction. *arXiv preprint arXiv:2008.08294*, 2020.
- [8] H. Tran, V. Le, and T. Tran. Goal-driven long-term trajectory prediction. In *Proceedings of the IEEE/CVF Winter Conference on Applications of Computer Vision*, pages 796–805, 2021.
- [9] J. Gu, C. Sun, and H. Zhao. Densetnt: End-to-end trajectory prediction from dense goal sets. In *Proceedings of the IEEE/CVF International Conference on Computer Vision*, pages 15303–15312, 2021.
- [10] P. Zhang, L. Bai, J. Xue, J. Fang, N. Zheng, and W. Ouyang. Trajectory forecasting from detection with uncertainty-aware motion encoding. *arXiv preprint arXiv:2202.01478*, 2022.
- [11] S. Casas, W. Luo, and R. Urtasun. Intentnet: Learning to predict intention from raw sensor data. In *Conference on Robot Learning*, pages 947–956. PMLR, 2018.
- [12] W. Luo, B. Yang, and R. Urtasun. Fast and furious: Real time end-to-end 3d detection, tracking and motion forecasting with a single convolutional net. In *Proceedings of the IEEE conference on Computer Vision and Pattern Recognition*, pages 3569–3577, 2018.
- [13] M. Liang, B. Yang, W. Zeng, Y. Chen, R. Hu, S. Casas, and R. Urtasun. Pnpnet: End-to-end perception and prediction with tracking in the loop. In *Proceedings of the IEEE/CVF Conference on Computer Vision and Pattern Recognition*, pages 11553–11562, 2020.
- [14] A. Hu, Z. Murez, N. Mohan, S. Dudas, J. Hawke, V. Badrinarayanan, R. Cipolla, and A. Kendall. Fiery: Future instance prediction in bird’s-eye view from surround monocular cameras. In *Proceedings of the IEEE/CVF International Conference on Computer Vision*, pages 15273–15282, 2021.
- [15] H. Caesar, V. Bankiti, A. H. Lang, S. Vora, V. E. Liong, Q. Xu, A. Krishnan, Y. Pan, G. Baldan, and O. Beijbom. nuscenes: A multimodal dataset for autonomous driving. In *Proceedings of the IEEE/CVF conference on computer vision and pattern recognition*, pages 11621–11631, 2020.
- [16] C. R. Qi, H. Su, K. Mo, and L. J. Guibas. PointNet: Deep Learning on Point Sets for 3D Classification and Segmentation. In *CVPR*, pages 652–660, 2017.
- [17] Y. Zhou and O. Tuzel. VoxelNet: End-to-End Learning for Point Cloud Based 3D Object Detection. In *CVPR*, pages 4490–4499, 2018.

- [18] A. H. Lang, S. Vora, H. Caesar, L. Zhou, J. Yang, and O. Beijbom. PointPillars: Fast Encoders for Object Detection from Point Clouds. In *CVPR*, pages 12697–12705, 2019.
- [19] A. Simonelli, S. R. Bulo, L. Porzi, M. López-Antequera, and P. Kotschieder. Disentangling monocular 3d object detection. In *Proceedings of the IEEE/CVF International Conference on Computer Vision*, pages 1991–1999, 2019.
- [20] T. Wang, X. Zhu, J. Pang, and D. Lin. Fcos3d: Fully convolutional one-stage monocular 3d object detection. *arXiv preprint arXiv:2104.10956*, 2021.
- [21] Y. Wang, W.-L. Chao, D. Garg, B. Hariharan, M. Campbell, and K. Q. Weinberger. Pseudo-LiDAR from Visual Depth Estimation: Bridging the Gap in 3D Object Detection for Autonomous Driving. In *CVPR*, pages 8445–8453, 2019.
- [22] Y. Wang, V. C. Guizilini, T. Zhang, Y. Wang, H. Zhao, and J. Solomon. Detr3d: 3d object detection from multi-view images via 3d-to-2d queries. In *5th Annual Conference on Robot Learning*, 2021.
- [23] Z. Li, W. Wang, H. Li, E. Xie, C. Sima, T. Lu, Q. Yu, and J. Dai. Bevformer: Learning bird’s-eye-view representation from multi-camera images via spatiotemporal transformers. *arXiv preprint arXiv:2203.17270*, 2022.
- [24] X. Weng, J. Wang, D. Held, and K. Kitani. 3D Multi-Object Tracking: A Baseline and New Evaluation Metrics. *IROS*, 2020.
- [25] Z. Pang, Z. Li, and N. Wang. Simpletrack: Understanding and rethinking 3d multi-object tracking. *arXiv preprint arXiv:2111.09621*, 2021.
- [26] X. Zhou, V. Koltun, and P. Krähenbühl. Tracking objects as points. In *European Conference on Computer Vision*, pages 474–490. Springer, 2020.
- [27] T. Yin, X. Zhou, and P. Krähenbühl. Center-based 3D Object Detection and Tracking. *arXiv preprint arXiv:2006.11275*, 2020.
- [28] S. Scheidegger, J. Benjaminsson, E. Rosenberg, A. Krishnan, and K. Granström. Mono-camera 3d multi-object tracking using deep learning detections and pmbm filtering. In *2018 IEEE Intelligent Vehicles Symposium (IV)*, pages 433–440. IEEE, 2018.
- [29] M. Chaabane, P. Zhang, J. R. Beveridge, and S. O’Hara. Deft: Detection embeddings for tracking. *arXiv preprint arXiv:2102.02267*, 2021.
- [30] H.-N. Hu, Y.-H. Yang, T. Fischer, T. Darrell, F. Yu, and M. Sun. Monocular quasi-dense 3d object tracking. *arXiv preprint arXiv:2103.07351*, 2021.
- [31] T. Zhang, X. Chen, Y. Wang, Y. Wang, and H. Zhao. Mutr3d: A multi-camera tracking framework via 3d-to-2d queries. In *Proceedings of the IEEE/CVF Conference on Computer Vision and Pattern Recognition*, pages 4537–4546, 2022.
- [32] J. Hong, B. Sapp, and J. Philbin. Rules of the road: Predicting driving behavior with a convolutional model of semantic interactions. In *Proceedings of the IEEE/CVF Conference on Computer Vision and Pattern Recognition*, pages 8454–8462, 2019.
- [33] R. A. Yeh, A. G. Schwing, J. Huang, and K. Murphy. Diverse generation for multi-agent sports games. In *Proceedings of the IEEE/CVF Conference on Computer Vision and Pattern Recognition*, pages 4610–4619, 2019.
- [34] C. Sun, P. Karlsson, J. Wu, J. B. Tenenbaum, and K. Murphy. Stochastic prediction of multi-agent interactions from partial observations. *arXiv preprint arXiv:1902.09641*, 2019.
- [35] Y. C. Tang and R. Salakhutdinov. Multiple futures prediction. *arXiv preprint arXiv:1911.00997*, 2019.
- [36] T. Gilles, S. Sabatini, D. Tsishkou, B. Stanciulescu, and F. Moutarde. Home: Heatmap output for future motion estimation. *arXiv preprint arXiv:2105.10968*, 2021.

- [37] T. Gilles, S. Sabatini, D. Tsishkou, B. Stanciulescu, and F. Moutarde. Thomas: Trajectory heatmap output with learned multi-agent sampling. In *International Conference on Learning Representations*, 2021.
- [38] H. Song, D. Luan, W. Ding, M. Y. Wang, and Q. Chen. Learning to predict vehicle trajectories with model-based planning. *arXiv preprint arXiv:2103.04027*, 2021.
- [39] B. Kim, S. H. Park, S. Lee, E. Khoshimjonov, D. Kum, J. Kim, J. S. Kim, and J. W. Choi. LaPred: Lane-aware prediction of multi-modal future trajectories of dynamic agents. In *Proceedings of the IEEE/CVF Conference on Computer Vision and Pattern Recognition*, pages 14636–14645, 2021.
- [40] M. Liang, B. Yang, R. Hu, Y. Chen, R. Liao, S. Feng, and R. Urtasun. Learning lane graph representations for motion forecasting. In *European Conference on Computer Vision*, pages 541–556. Springer, 2020.
- [41] J. Phillips, J. Martinez, I. A. Barsan, S. Casas, A. Sadat, and R. Urtasun. Deep multi-task learning for joint localization, perception, and prediction. In *Proceedings of the IEEE/CVF Conference on Computer Vision and Pattern Recognition (CVPR)*, pages 4679–4689, June 2021.
- [42] F. Zeng, B. Dong, T. Wang, X. Zhang, and Y. Wei. Motr: End-to-end multiple-object tracking with transformer. *arXiv preprint arXiv:2105.03247*, 2021.
- [43] K. He, X. Zhang, S. Ren, and J. Sun. Deep Residual Learning for Image Recognition. In *CVPR*, pages 770–778, 2016.
- [44] T.-Y. Lin, P. Dollár, R. Girshick, K. He, B. Hariharan, and S. Belongie. Feature Pyramid Networks for Object Detection. In *CVPR*, pages 2117–2125, 2017.
- [45] N. Carion, F. Massa, G. Synnaeve, N. Usunier, A. Kirillov, and S. Zagoruyko. End-to-end object detection with transformers. In *ECCV*, 2020.
- [46] J. Gao, C. Sun, H. Zhao, Y. Shen, D. Anguelov, C. Li, and C. Schmid. Vectornet: Encoding hd maps and agent dynamics from vectorized representation. In *Proceedings of the IEEE/CVF Conference on Computer Vision and Pattern Recognition*, pages 11525–11533, 2020.
- [47] H. Cui, V. Radosavljevic, F.-C. Chou, T.-H. Lin, T. Nguyen, T.-K. Huang, J. Schneider, and N. Djuric. Multimodal trajectory predictions for autonomous driving using deep convolutional networks. In *2019 International Conference on Robotics and Automation (ICRA)*, pages 2090–2096. IEEE, 2019.
- [48] C. Rupprecht, I. Laina, R. DiPietro, M. Baust, F. Tombari, N. Navab, and G. D. Hager. Learning in an uncertain world: Representing ambiguity through multiple hypotheses. In *Proceedings of the IEEE international conference on computer vision*, pages 3591–3600, 2017.
- [49] T. Gilles, S. Sabatini, D. Tsishkou, B. Stanciulescu, and F. Moutarde. Gohome: Graph-oriented heatmap output for future motion estimation. *arXiv preprint arXiv:2109.01827*, 2021.
- [50] M.-F. Chang, J. Lambert, P. Sangkloy, J. Singh, S. Bak, A. Hartnett, D. Wang, P. Carr, S. Lucey, D. Ramanan, et al. Argoverse: 3d tracking and forecasting with rich maps. In *Proceedings of the IEEE/CVF Conference on Computer Vision and Pattern Recognition*, pages 8748–8757, 2019.

A Implementation Details

Query-based Tracker. The query-based tracker takes ResNet50 [43] as the image backbone and DETR3D [22] as the detection head. The detection head consists of 6 layers, and each layer contains a feature refinement layer and a multi-head attention layer with layer normalization. The hidden size for the detection head is set to 256. Finally, one branch predicts center coordinates and size of agents, and the other branch predicts agent type.

Trajectory Predictor. Popular trajectory prediction benchmarks, such as Argoverse Motion Prediction Benchmark [50], require the prediction of one target agent in each scene. A commonly used trick is to normalize the map and the agent trajectories by taking the last position of the target agent as the origin and its direction as y -axis. This normalization makes prediction models focus on future modality prediction instead of coordinate transformation, thereby improving the prediction performance but limited to predicting one agent at a time. In our visual trajectory prediction task, we simultaneously predict all agents in each scene for a fast inference speed. Although we cannot normalize the maps and the surrounding agents for each target agent, we can predict the offsets between the future trajectories and the current position of the target agent.

Training and Inference Details. In our experiments, all models are trained on the nuScenes training set with a batch size of 8 for 24 epochs. The Adam optimizer is adopted to train the whole pipeline. The learning rate has an initial value of $2e^{-4}$ and decays to 10% at the 20th and the 23rd epochs. The hidden size of the query-based tracker is set to 256, and that of the trajectory decoder is set to 128. We evaluate all models on the nuScenes validation set. All models are tested online by feeding raw data of each time step to the model in chronological order. The metric computing is performed at every step except for steps that do not have enough future frames. Unlike popular trajectory prediction benchmarks requiring the prediction of selected agents, we simultaneously predict all agents at each step.

B Trajectory Decoder

ViP3D can leverage a variety of trajectory decoding methods, such as regression-based methods [4, 47, 48, 40], goal-based methods [7] and heatmap-based methods [9, 36, 49]. We conduct experiments on these three trajectory decoding methods. In this section, we introduce the implementation details of these methods.

Regression-based. The regression-based trajectory decoder is a 2-layer MLP that takes the agent queries as input and directly outputs multiple future trajectories. During inference, the regression-based trajectory decoder directly outputs a set of predicted trajectories. During training, we first calculate the distance between each predicted trajectory \hat{s} and ground truth trajectory s : $d(s, \hat{s}) = \sum_{t=1}^{T_{\text{future}}} \|s_t - \hat{s}_t\|$, where $\|\cdot\|$ is the ℓ_2 distance between two points. Then, we select the predicted trajectory with the closest distance: $\hat{k} = \operatorname{argmin}_{k \in 1 \dots K} d(s, s^{(k)})$, where $s^{(k)}$ is the k^{th} predicted trajectory. Finally, we calculate regression loss between the closest predicted trajectory $s^{(\hat{k})}$ and the ground truth trajectory s as

$$\mathcal{L}_{\text{trajectory}} = \sum_{t=1}^{T_{\text{future}}} \mathcal{L}_{\text{reg}}(s_t, s_t^{(\hat{k})}), \quad (4)$$

where \mathcal{L}_{reg} is the smooth ℓ_1 loss between two points.

Goal-based. The goal-based trajectory decoder consists of a goal encoder, a probability decoder, an offset decoder, and a trajectory completion module. These modules are implemented using MLP. For each agent, we first randomly generate a set of candidate goals. The goal encoder is used to obtain the features of candidate goals by taking their coordinates as input. After that, a concatenation of the agent query and the features of goal coordinates is fed into the probability decoder and offset decoder. The probability decoder and the offset decoder output predicted goal probabilities and goal offsets, respectively. Let \mathcal{L}_{cls} be the binary cross-entropy loss for the probability decoder,

and let \mathcal{L}_{reg} be the smooth ℓ_1 loss for the offset decoder. To obtain K trajectories, Non-maximum supervision (NMS) is employed to select K goals (after adding the goal offsets), and the trajectory completion module takes the K selected goals and outputs K trajectories. Let $\mathcal{L}_{\text{completion}}$ be the smooth ℓ_1 loss for the trajectory completion module. Then the overall loss is

$$\mathcal{L}_{\text{trajectory}} = \mathcal{L}_{\text{cls}} + \mathcal{L}_{\text{reg}} + \mathcal{L}_{\text{completion}}. \quad (5)$$

Heatmap-based. The heatmap-based trajectory decoder only consists of a goal encoder, a probability decoder, and a trajectory completion module. These modules are implemented using MLP. For each agent, to obtain a heatmap indicating the probability distribution of the final positions of the trajectories, we first densely sample goals with a sampling density of 1m. The goal encoder is used to obtain the features of the goals by taking the their coordinates as input. After that, a concatenation of the agent query and the features of goal coordinates is fed into the probability decoder. The probability decoder outputs predicted goal probabilities, and we obtain the heatmap. Let \mathcal{L}_{cls} be the binary cross-entropy loss for the probability decoder. To obtain K trajectories, we also use NMS to select K goals for simplification, instead of using greedy algorithms as in origin heatmap-based methods [36]. The trajectory completion module takes the K selected goals and outputs K trajectories. Let $\mathcal{L}_{\text{completion}}$ be the smooth ℓ_1 loss for the trajectory completion module. Then the overall loss is

$$\mathcal{L}_{\text{trajectory}} = \mathcal{L}_{\text{cls}} + \mathcal{L}_{\text{completion}}. \quad (6)$$

C Qualitative Results

We show more visualizations of detected agents with their predicted trajectories obtained by our ViP3D, as shown in Figure 4. These visualizations include motion prediction for both vehicles and pedestrians in different scenarios. Based on vision inputs, our ViP3D can predict reasonable future trajectories.

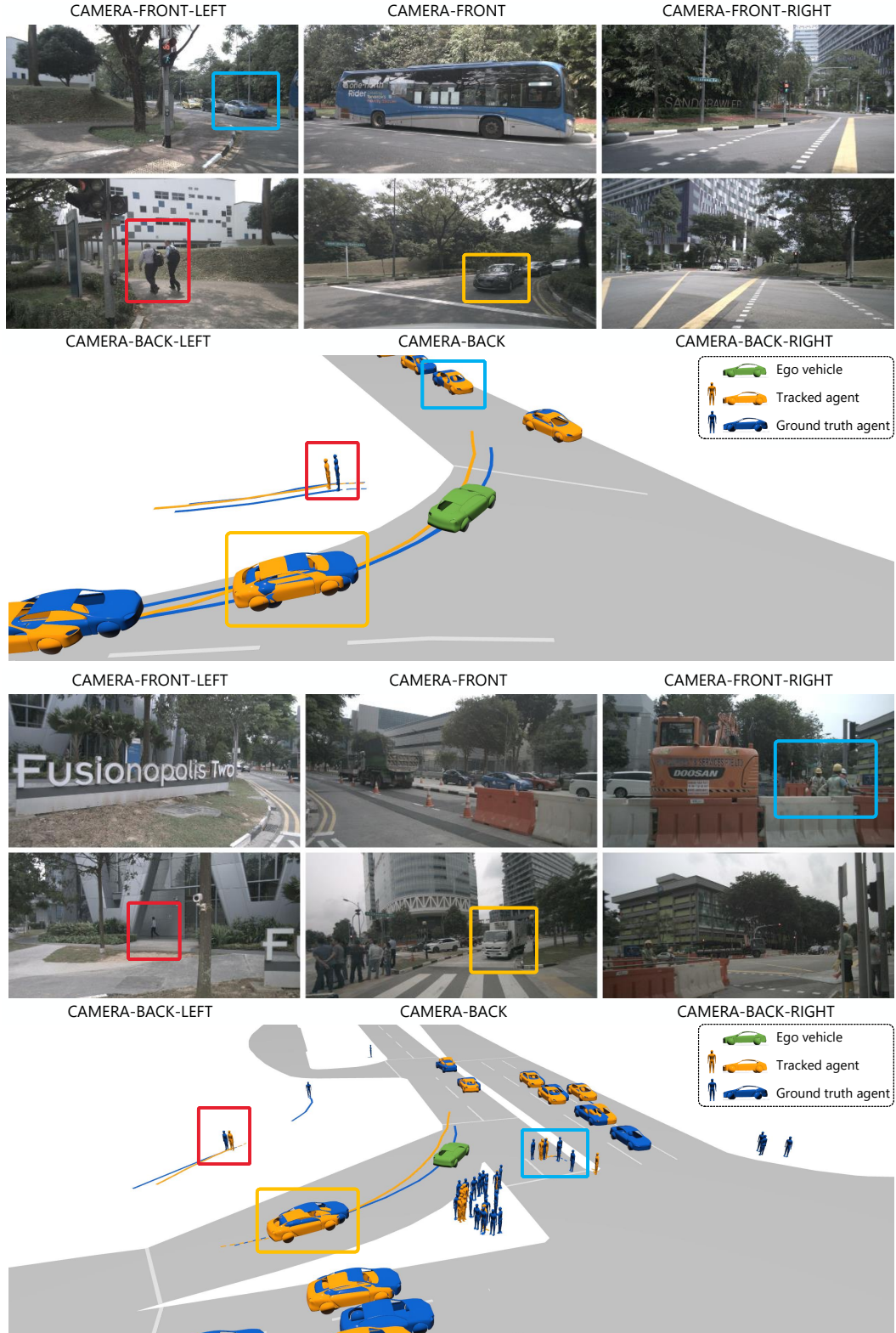


Figure 4: Qualitative results of ViP3D for end-to-end trajectory prediction. Agents with the same identity are enclosed by boxes of the same color. The green vehicle is the ego agent. The blue and orange agents indicate ground-truth and tracked agents, respectively. The blue and orange curves indicate ground-truth and predicted future trajectories of agents, respectively. For each agent, only the predicted trajectory with the highest probability is drawn.